Generation of high-order harmonics in a self-guided beam

V. Tosa,* E. Takahashi, Y. Nabekawa, and K. Midorikawa[†]

Laser Technology Laboratory, RIKEN, 2-1 Hirosawa, Wako, Saitama 3510198, Japan
(Received 26 July 2002; published 30 June 2003)

Generation of high-order harmonics in Xe was studied in a static cell at high pump energies, 5 m focal length, and up to 14 cm interaction lengths. Self-guided propagation of the pulse was observed experimentally and confirmed by a three-dimensional model. Phase-matched generation was demonstrated in the self-guided beam, and the high energy and low divergence of the harmonic radiation were explained. Harmonic field calculations, in good agreement with experimental results, allow for the explanation of the higher-order harmonic generation dynamics in the self-guided region.

High-order harmonic generation (HHG) [1,2] has been studied extensively during the past years, since it represents a unique source of radiation with practical applications. A large effort is devoted to increase the number of photons emitted per pulse, since many additional applications would become possible. An approach worth mentioning is [3,4] the phase-matched (PM) guided wave technique, using a gas-filled optical fiber system. Recent advances [5] report a 10^3 enhancement of the PM harmonic yield compared to the non-PM case. For the free-space case, the focusing geometry, the gas position relative to the laser focus, as well as their influence on the PM have been key issues in HHG optimization. Tamaki *et al.* [6] reported a high conversion efficiency in Ne, and attributed it to the formation of a self-guided (SG) beam. High conversion efficiency was also reported in Ar [7] under loose focusing geometry. Experiments in Xe under strong ionization conditions [8] have revealed a weak maximum for the gas placed in the diverging beam and a strong one when the gas was placed in the converging beam. A recent report [9] found only one maximum for the Xe jet located in the converging beam. To explain these results, in contradiction with PM predictions [10], both works *assumed* that, when focused after the jet, the laser convergence is reduced, resulting in a uniform phase and an intensity distribution due to *channeling*. However, until now, no correlated measurements of both SG beam formation and HHG have been reported. The formation of the channel in air and then its use in a static cell [11] demonstrated quasiphase matching for the third harmonic (H3) in Xe.

In this paper, we report results on HHG in a SG pump beam which is formed in Xe gas, and demonstrate that PM generation of harmonics depends essentialy on SG formation. Focusing high (10–20 mJ) pulse energies on a static cell which, unlike the jet case [8,9], secure a uniform gas distribution over long (4–14 cm) interaction lengths is the key factor for the SG formation. Correlated measurements of plasma fluorescence and harmonic yield revealed that when the SG sets in, the harmonic yield is greatly enhanced. Fluorescence intensity along the propagation coordinate is in

good agreement with the electron concentration, calculated in a three-dimensional (3D) model. Coherence lengths in the SG region exceed the cell length, meaning that harmonics build up under PM conditions. Calculations of the harmonic field reproduce well the experimental data, and confirm the PM regime in the SG beam.

The experiment was carried out with a 10 Hz Ti:sapphire laser system based on chirped pulse amplification. A pulse of 35 fs and wavelength centered at 810 nm was loosely focused by a $f = 5$ m fused silica plane convex lens, and delivered into the chamber through a CaF_2 window. The interaction cell had two (1.5 mm diameter) pinholes on each end surface, isolating the vacuum and gas-filled regions. Gas pressure in the interaction cell can be finely adjusted and measured. A window placed perpendicular to the beam propagation, allows one to observe the interaction region. The generated harmonics illuminated a 150 μm $\times$ 25 mm slit of the flat-field normal-incidence extreme ultraviolet (XUV) spectrometer with a platinum-coated concave grating blazed at 60 nm (1200 lines/mm). This spectrometer, equipped with a microchannel plate (MCP), can cover the spectral range from 30 to 80 nm. A charge-coupled device camera detected two-dimensional fluorescence from a phosphor screen placed behind the MCP. Therefore, we measured spectrally resolved far-field profiles of high-order harmonics. Harmonics from H11 to H19 were measured, however, we tried to optimize harmonic H13 as a SiC mirror, having high reflectivity at normal incidence, available in the wavelength region longer than 62 nm. The absolute energy was measured directly (see Ref. [12] for details) with an unbiased silicon XUV photodiode (XUV-100), which was inserted in front of the spectrometer and the output signal was recorded directly on an oscilloscope.

During experiments, the plasma fluorescence was usually observed as a uniform light column. When the cell is placed in the converging beam, as in Fig. 1(a), the intensity of the fluorescence has a slow z variation with a loose maximum located within the cell length. For the cell placed in the diverging beam, i.e., with the input pinhole after the focus, the fluorescence intensity decreased uniformly from the input towards the output pinhole [see Fig. 1(b)], and the harmonic yield decreased considerably. The transition between these two opposite cases is continuous. The fluorescence intensities along the propagation coordinate are in good agreement

_____

*On leave from National Institute for R&D in Isotopic and Molecular Technologies, Cluj-Napoca, Romania.

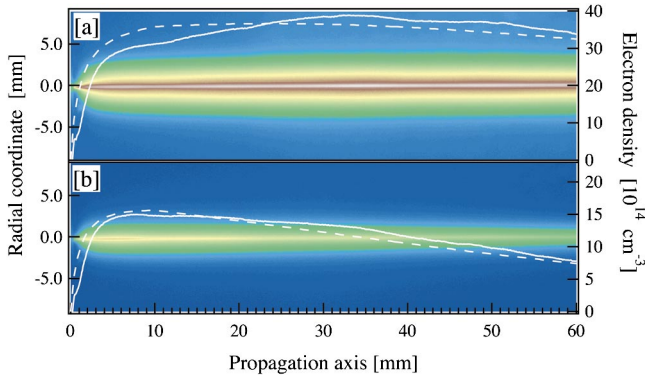[†]Electronic address: kmidori@postman.riken.go.jp

FIG. 1. (Color) The plasma fluorescence along the propagation coordinate, in 0.6 torr of Xe at 10 mJ pump energy, for a 14 cm cell (a) placed in the converging beam at $z_L = 24$ cm, and (b) placed in the diverging beam at $z_L = -20$ cm. Fluorescence intensities (solid lines, same arbitrary units in the two cases), as well as calculated electron concentration (dashed line, cm^{-3}) are also shown. Technically only 6 cm can be measured.

with the electron concentrations, calculated as described below, and also shown in Fig. 1.

The experimental results have been analyzed in terms of a 3D nonadiabatic propagation model. In an ionized gas, the pulse evolution is described by the wave equation, which can be written as [13]

$$\nabla^2 E_1 - \frac{1}{c^2} \frac{\partial^2 E_1}{\partial t^2} = \frac{\omega_1^2}{c^2} (1 - n_{eff}^2) E_1, \quad (1)$$

where $E_1(r,z,t)$ is the axially symmetric transverse electric field of frequency ω_1. The effective refractive index of the medium was written as $n_{eff}(r,z,t) = n_0(r,z,t) + n_2 I(r,z,t) - \omega_p^2(r,z,t)/2\omega_1^2$. The linear term $n_0 = 1 + \delta_1 - i\beta_1$ accounts for the refraction (δ_1) and absorption (β_1), while the second term describes the optical Kerr effect. The third term contains the plasma frequency $\omega_p = (4\pi e^2 \rho_e / m)^{1/2}$ and ac-
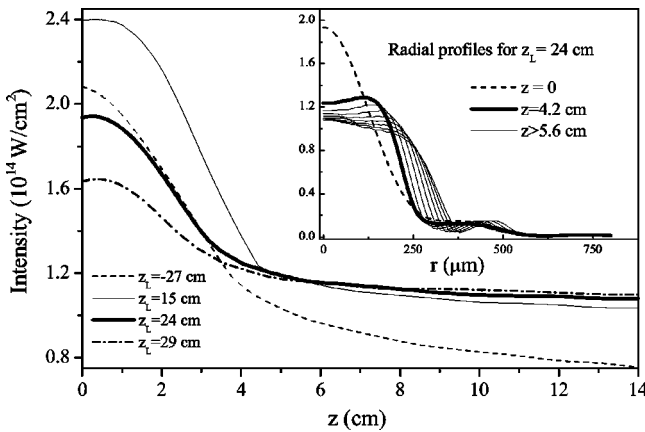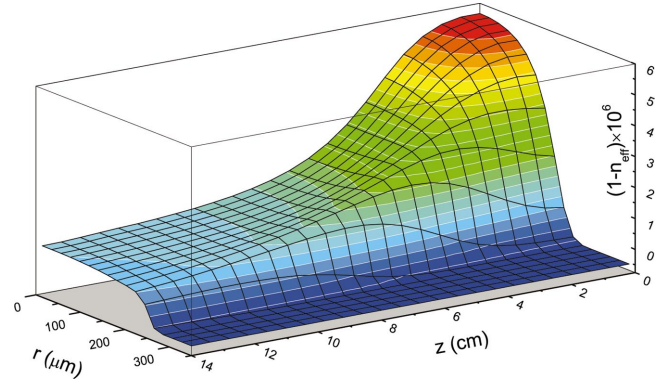

FIG. 3. (Color) The effective refraction index in the interaction region for $z_L = 24$ cm, other conditions as in Fig. 2. For convenience, the quantity $(1 - n_{eff}) \times 10^6$ was plotted.

counts for the presence of a density ρ_e of electrons per unit volume. The free-electron generation was calculated either by Ammosov-Delone-Krainov (ADK) formula [14], in the tunneling regime, or by using the rates calculated by Kulander [15] for the valence p shell of Xe, in the multiphoton regime. The method used to solve Eq. (1) is fully described in Ref. [16]. As the right-hand term contains the solution, we followed an iterative self-consistent procedure at each step of integration.

We used the *measured* energy and duration of the pulse to calculate the peak intensity and the initial field values for the propagation equation. Shown in Fig. 2 is the on-axis field calculated for a peak intensity of 2.7×10^{14} W/cm^2, 0.6-torr gas in a 14-cm-long cell, and for different positions z_L of the input pinhole with respect to the focus. After an initial decrease, the intensity remains almost constant for the remaining of the propagation distance. When this happens, the radial profile of the intensity becomes nearly tophat, as also shown in Fig. 2. Thus, for $z \geq 5-6$ cm the intensity remains almost constant in a cylinder of about 250 μm radius. For

FIG. 2. Calculated on-axis intensity in the cell for different positions z_L of the input pinhole relative to the focus. Pozitive z_L means input pinhole before the focus. The inset shows the radial profiles for $z_L = 24$ cm.
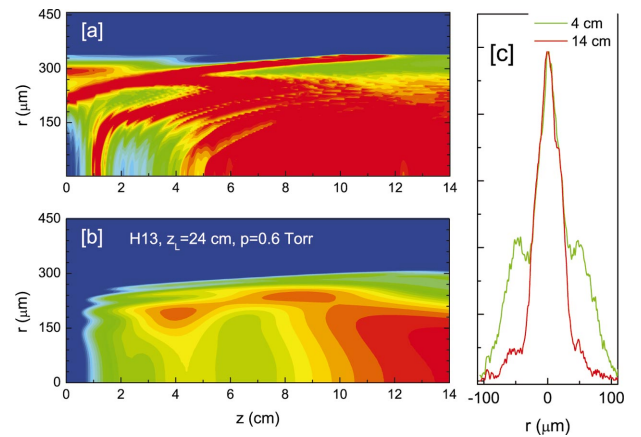

FIG. 4. (Color) (a) Calculated harmonic H13 coherence length map. Blue regions have $L_{coh} \leq 1$ cm and red regions have $L_{coh} \geq 14$ cm. (b) Calculated harmonic H13 near-field intensity map, arbitrary units. Red:blue ratio $\approx 50:1$. (c) Normalized harmonic H13 radial profiles, measured for 4 cm and 14 cm cell lengths.

$z_L > 0$, this constant intensity is practically independent of z_L. The phase of the fundamental follows closely the behavior of the intensity: a rapid initial decrease is followed by a fairly constant phase in the SG part. Similar field configurations were generated for all cases in which the cell was placed in the converging beam. For negative z_L, these features gradually disappear, as seen in Fig. 1 for $z_L = -20$ cm.

Channeling occurs [13] as a balance between the Kerr self-focusing and the electron defocusing. However, in our range of pressures and field intensities, the Kerr contribution to the refractive index is small compared to that given by the electrons. At first sight, it seems unlikely that the ionization nonlinearity alone, without any focusing counterpart, can be a sufficient mechanism for SG, an ultrashort laser pulse. However, our data show that the ionization profile formed initially, when the pulse enters the gas medium, acts like a diverging lens with decreasing focal power as r increases. Therefore, the initial convergent wave front changes its radius of curvature, more in the central and less in the peripheral regions. In particular, this radius of curvature becomes infinite when the following condition [17] is satisfied: $\omega_p^2/\omega_1^2 = \lambda^2/\pi^2 w_0^2$, where w_0 is the beam waist size and λ is the wavelength. For our case $\lambda^2/\pi^2 w_0^2 = 1.1 \times 10^{-6}$ for $w_0 = 250$ μm, while from the data in Fig. 3 it results that in the SG region ω_p^2/ω_1^2 decreases from 1.5×10^{-6} for $z = 6$ cm down to 0.8×10^{-6} for $z = 14$ cm. It follows that in this region the laser beam propagates like a plane wave in a cylinder of a well-defined radius, which is set by the sharp increase of the refractive index, as seen in Fig. 3. As early anticipated by Rankin [17], and later confirmed by computer calculations [18,19], such a distribution can guide an electromagnetic wave in the form of a leaking mode with exponentially small losses over distances of many free Rayleigh lengths. As distinct from the common SG effect, where the field confinement is due to the total internal reflection at the guide boundaries, in this case the effect is obtained due to a strong reflection of the trapped wave from the plasma boundary that is sharp as compared to the transverse scale.

The ionization level in the channel sets the value for the field intensity, which will basically depend on the ionization rate of the atom. This intensity will be lower than the saturation intensity (as it does not produce full ionization but about 20% in our case) and this is particularly favorable for HHG. An intensity close to the saturation threshold will yield a weak harmonic signal as most of the atoms will only be ionized, while an intensity close to the ionization threshold will induce weak polarization, thus again decreasing the overall yield. A certain degree of ionization is thus necessary and, in fact, it represents a fundamental ingredient for HHG.

A PM analysis performed by using the graphical method of Balcou *et al.* [10] shows that the channel formation is essential for a good PM. For harmonic H13, we calculated the polarization wave vector as $\mathbf{k}_{pol} = 13\nabla[\phi_1(r,z)] + \nabla[\alpha I(r,z)]$, where ϕ_1 is the fundamental field phase and α the phase coefficient [20] for harmonic H13 generated in the plateau. Following Ref. [10] we define a coherence length $L_{coh} = \pi/\delta k$, where $\delta k = 2\pi q/\lambda - |\mathbf{k}_{pol}|$. We want to

point out that $I(r,z)$ and $\phi_1(r,z)$ are here obtained from the calculated solution of the propagation equation and *not* from the unperturbed fundamental field. The advantage of this procedure, which to the best of our knowledge is applied here for the first time, is that all the nongeometrical effects (dispersion, absorption, and ionization) are already included in L_{coh}, thus, one does not need to consider them separately as is done usually.

For $z_L = 24$ cm case of Fig. 2, we present in Fig. 4(a) the calculated L_{coh} map for harmonic H13. As one can note, in the SG beam, that is for $z > 5$ cm and $r < 250$ μm, we have $L_{coh} > 14$ cm, thus harmonic H13 develops under PM conditions. The PM region has a large volume, which is the main reason for the high conversion efficiency [12] obtained in our experiments. The PM region is spatially compact and located around the propagation axis. This explains the low divergence of the generated harmonics in optimized conditions.

For the harmonic field calculation, the single-atom response, estimated in the strong field approximation (SFA) [21] formalism, is the source term for a 3D propagation code, as described in Ref. [16]. Atomic dispersion and absorption terms are also included. From the near-field solution we calculated the far-field using a Hankel transform [22]. The near-field (r,z) map of harmonic H13 is presented in Fig. 4(b). It follows closely the L_{coh} map, which substantiate our PM calculation. It also shows the transition from an off-axis, unoptimized emission for $z = 4$ cm to an on-axis emission for $z = 14$ cm, when the harmonic H13 field is optimized. Indeed, for a 4 cm cell, see Fig. 4(c), the measured radial profiles show one central peak with lateral wings. The wings contain 37% of the total energy, indicating off-axis emission. For a 14-cm cell, only 8% of the energy is in the weak wings, and 92% in the peak. In these latter case, both the measured [12] and the calculated divergence of harmonic H13 are around 0.5 mrad.

Presented in Fig. 5 is the dependence of harmonic H13 yield on z_L. A large distribution is obtained, with the maximum located around $z_L = 27$ cm. The harmonic H13 energy attained, measured as described in Refs. [7,12], was as high
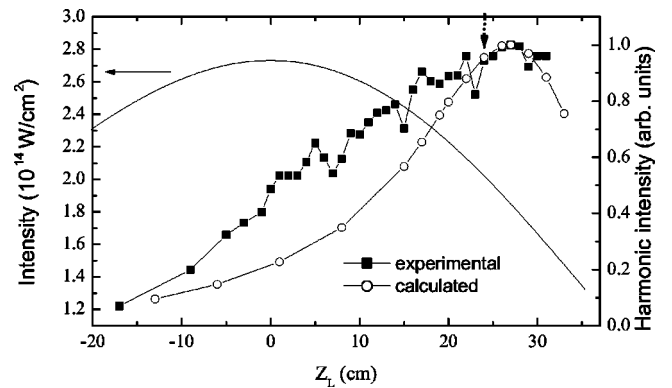

FIG. 5. The harmonic H13 yield dependence on z_L, for 10 mJ/pulse, 13.5 mm aperture diameter, 0.6 torr Xe pressure. The experimental data were shifted along z_L to bring the two maxima in coincidence. The vertical arrow shows the z_L position for which pressure and length dependence experiments were performed. On-axis intensity for the unperturbed beam is also shown.
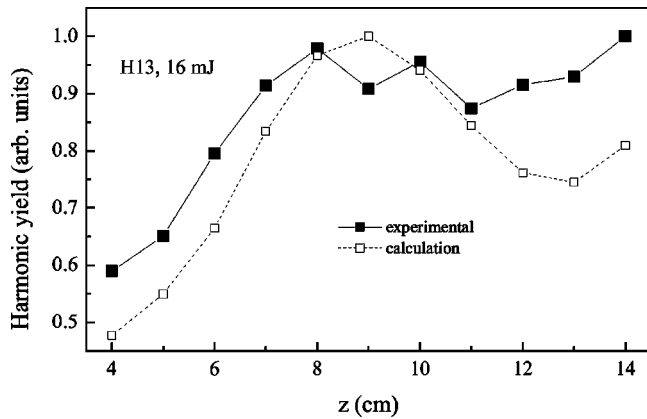
FIG. 6. Dependence of the harmonic H13 yield on cell length for a pulse energy of 16 mJ. Other conditions as in Fig. 5.

as 4.7 μJ with an almost perfect spatial profile, as seen in Fig. 4(c) and also reported in Ref. [12]. The computed curve, also presented in Fig. 5, has a narrower distribution along the z_L coordinate. This is probably due to the nonideal distribution of the real beam intensity and phase along the propagation axis. For $z_L > 0$, the increase of the yield is due to the increase of the SG length towards the input pinhole. The decrease after $z_L = 27$ cm is due to the pump intensity decrease which produces field oscillations towards output pinhole. When the cell is placed after the focus (negative z_L), the harmonic yield declines. The smaller the z_L is, the greater the phase and intensity variation are along r and z. This induce a smaller coherence length, and, in turn, poorer harmonic yield. A calculation performed at 7 mJ pulse energy yielded the maximum about 2 cm closer to the focus. This indicates that both initial intensity and wave front radius of

curvature combine to yield an optimized SG field configuration.

For the conditions specified in Fig. 5 and a pulse energy of 16 mJ, we plotted in Fig. 6 the harmonic H13 yield as a function of cell length. The length was varied between 4 cm and 14 cm, keeping constant the input pinhole position. Periodic oscillations of the harmonic yield with cell length are expected [11] for PM harmonics. However, absorption add a dumping factor to these oscillations. If we switch off the absorption in our model, we obtain curves which, with the increasing cell length, increase much faster than the data in Fig. 6. We thus conclude that absorption plays a crucial role in limiting the increase of the harmonic yield and in fixing the optimum cell length.

We should add that both the fiber guided wave technique [3–5] and the SG method presented here search for a pump beam configuration which ensures PM HHG over distances greater than 2–3 characteristic absorption lengths. This is achieved, in both cases, by creating a uniform gas distribution though which the pump beam is guided. Our method allows for, unlike the fiber guided case, high input energies, and, more important, up scaling of the spatial coordinates [7,12], which keep open the possibility of increasing the output energy.

In conclusion, we presented experimental and calculated results concerning HHG in a SG beam. The formation of the SG beam, without Kerr self-focussing, was evidenced experimentally and confirmed by a 3D propagation model. Inside the SG beam, which propagate like a plane wave in a confined cylinder, harmonics are generated under PM conditions, the conversion efficiency being limited only by the absorption. The dependence of the harmonic yield on the experimental parameters was explained and well reproduced by calculations.

[1] P. Salières *et al.*, Adv. At., Mol., Opt. Phys. **41**, 83 (1999).
[2] T. Brabec and F. Krausz, Rev. Mod. Phys. **72**, 545 (2000).
[3] Y. Tamaki *et al.*, Phys. Rev. A **59**, 4041 (1999).
[4] C. Durfee *et al.*, Phys. Rev. Lett. **83**, 2187 (1999).
[5] A. Rundquist *et al.*, Science **280**, 1412 (1998).
[6] Y. Tamaki *et al.*, Phys. Rev. Lett. **82**, 1422 (1999).
[7] E. Takahashi *et al.*, Phys. Rev. A **66**, 021802 (2002).
[8] M. Bellini *et al.*, Phys. Rev. A **64**, 023411 (2001).
[9] J.-F. Hergot *et al.*, Phys. Rev. A **66**, 021801 (2002).
[10] P. Balcou *et al.*, Phys. Rev. A **55**, 3204 (1997).
[11] H.R. Lange *et al.*, Phys. Rev. Lett. **81**, 1611 (1998).
[12] E. Takahashi *et al.*, Opt. Lett. **27**, 1920 (2002).

[13] E. Esarey *et al.*, IEEE J. Quantum Electron. **33**, 1879 (1997).
[14] M. Amosov *et al.*, Zh. Eksp. Teor. Fiz. **91**, 2008 (1986) [Sov. Phys. JETP **64**, 1191 (1987)].
[15] K.C. Kulander, Phys. Rev. A **38**, 778 (1988).
[16] E. Priori *et al.*, Phys. Rev. A **61**, 063801 (2000).
[17] R. Rankin *et al.*, Opt. Lett. **16**, 835 (1991).
[18] A. Sergeev *et al.*, Laser Part. Beams **17**, 129 (1999).
[19] V. Gildenburg *et al.*, Phys. Rev. E **63**, 066402 (2001).
[20] M. Lewenstein *et al.*, Phys. Rev. A **52**, 4747 (1995).
[21] M. Lewenstein *et al.*, Phys. Rev. A **49**, 2117 (1994).
[22] E. Siegman, *Lasers* (University Sciences, Mill Valey, CA, 1986).